Chapter 6
Conformational Dynamics of A30G α-Synuclein that causes familial Parkinson disease

Conformational Dynamics of A30G α-Synuclein that causes familial Parkinson disease

6.1. Abstract:

The first gene shown to be responsible for autosomal-dominant PD is the SNCA gene, which encodes for α-Syn. Recently, a novel heterozygous A30G mutation of the SNCA gene associated with familial PD has been discovered and the clinical features of affected patients, genetic findings, and functional consequences have been reported. However, little research has been done on how the A30G mutation affects the structure of α-Syn. So, using atomistic MD simulation, we here highlight the key structural characteristics of A30G α-Syn in the free monomer form and membrane associated state. From the MD trajectory analysis, the structure of A30G α-Syn was noticed to undergo rapid change in conformations and to have higher backbone flexibility near the site of mutation and decrease in α-helical propensity. The typical torsion angles in certain residues (Val26 and Glu28) near the mutation site were observed to deviate significantly in A30G α-Syn in its free form as well in the membrane bound form. In the case of membrane bound A30G α-Syn, the regions that were submerged in the lipid bilayer (N-helix (3-37) and turn region (38-44)) found to contain higher helical content than the elevated region above the lipid surface. The bending angle in the helix-N and helix-C regions were noticed to be relatively higher in the free form of A30G α-Syn (38.5º) than in the membrane bound form (37º). The A30G mutation in α-Syn was predicted to have an impact on the stability and functionality of the protein based on ΔΔG values obtained from the online servers. Our results demonstrate that the A30G mutation in α-Syn altered the protein's α-helical structure and slightly altered the membrane binding.

6.2. Introduction:

PD is the most common movement disorder and the second-most prevalent neurodegenerative disease, and it is marked by a number of non-motor symptoms in addition to its cardinal motor symptoms [413]. Degeneration of nigrostriatal dopaminergic neurons and the widespread development of Lewy bodies, aberrant neuronal cytoplasmic inclusions primarily made of aggregated α-Syn, a widely expressed protein produced by the SNCA gene, are the clinical hallmarks of PD [414-417]. Seven distinct missense mutations (A30P, E46K, H50Q, G51D, A53T, A53E, and A53V) have been found to be linked to PD [418,419], and SNCA was the first gene to be identified as causing autosomal dominant PD [127,160,335,420-428]. Among the seven distinct missense mutations, the A53T mutation was the first missense mutation

found in SNCA and most common in families with Greek or Italian roots [25]. In case of H50Q mutation, since there was no evident case of PD as compared to controls in large databases, so it was considered to be not pathogenic [429-434]. Other SNCA missense mutations (E46K [157, 435], G51D [436, 437] and A53E [158,438]) have been identified in a number of families and/or cases, but A30P was only discovered to co-segregate in five affected individuals of one German family [439] Many other studies have highlighted that multiple amino acid substitutions at the position 30 in WT α-Syn may represent a potential pathological site in association with PD [155, 440-445]. In a recent study, five affected people from three unrelated Greek families were found to have a new heterozygous A30G mutation of the SNCA gene where the clinical, functional characteristics and genetic findings of A30G mutation were discussed [23]. Therefore, a thorough understanding of the structural characteristics of A30G α-Syn in its membrane-associated state will undoubtedly offer an insight on how this protein carries out its normal function. Today, there are numerous in-silico methods available to comprehend how point mutations affect a protein's functional and structural dynamics [446-456].

The conformational dynamics of A30G α-Syn as a free monomer in solution and as a monomer associated with a lipid membrane were investigated in this study. Our findings show that the N-terminal of α-Syn attaches to the lipid membrane and adopts an expanded helical configuration, whereas the C-terminal of the α-Syn protein remains free and open to potential interactions with other proteins. The structure of A30G α-Syn in solution as a free monomer was noticed to be mostly unfolded, but it did show a preference for helical conformation, which may be important in the aggregation of α-Syn into fibrils.

6.3. Materials and methods:

6.3.1. Construction of A30G α-Synuclein:

The initial structure of A30G α-Syn mutant for the MD simulation study was obtained by modifying the 3D structure of human micelle-bound WT α-Syn (PDB ID: 1XQ8). The 3D structure of WT α-Syn was retrieved from the Protein Data Bank [457]. The Rotamer tool of the University of California, San Francisco CHIMERA software [306] was used to construct A30G α-Syn, where Alanine was replaced with Glycine at position 30 in the WT α-Syn.

6.3.2. Simulation of A30G α-Synuclein as a free monomer in solution:

The MD simulation was performed by using the Particle Mesh Ewald MD module [337, 338] of the AMBER 18 simulation package [205] with force field ff99SBildn [227]. The mutant A30G α-Syn was created from the WT α-Syn using UCSF Chimera [306]. In the free monomer

state, the A30G α-Syn was simulated in explicit solvent and solvated with the TIP3P [212] water model with a solvent buffer of 10 Å in all directions. Appropriate numbers of counter ions were supplied to the A30G α-Syn system to ensure overall neutrality of the system. For handling long range electrostatic interactions, the Particle Mesh Ewald method [337] was utilized, and for treating short range non-bonded interactions, a force shifted cut-off of 8.0 Å was employed. Hydrogen atoms were held in an equilibrium state. The SHAKE method was used to limit the hydrogen atoms to the equilibrium bond length [203]. To eliminate undesirable van der Waals interactions, the system was subjected to 1000 steps of steepest descent minimization, followed by 4000 steps of conjugate gradient minimization, with the protein bound by a 500 kcal/mol harmonic potential. Then, using 10,000 steepest descent minimization steps without harmonic restrictions, the entire systems (protein and water) were reduced. The A30G α-Syn system was then gradually heated from 0-300 K in NVT conditions, with harmonic constraints applied to the solute atoms with a force constant of 10 kcal/mol, and equilibration was performed three times with 3000 ps using a force constant of 5.0 kcal/mol. The equilibration was conducted in NPT conditions (300 K and 1 atm pressure) for 2 ns. To ensure successful equilibration and stabilisation of the system, the temperature, energy and pressure graphs were plotted and analysed as shown in **Figure 6.1**. Following the equilibration step, the production runs were carried out for 100 ns with a 1 fs time step and with an NPT ensemble. The coupling constants of the Berendsen thermostat and barostat were 1.0 and 2.0 ps, respectively, which were used to regulate temperature and pressure [343].

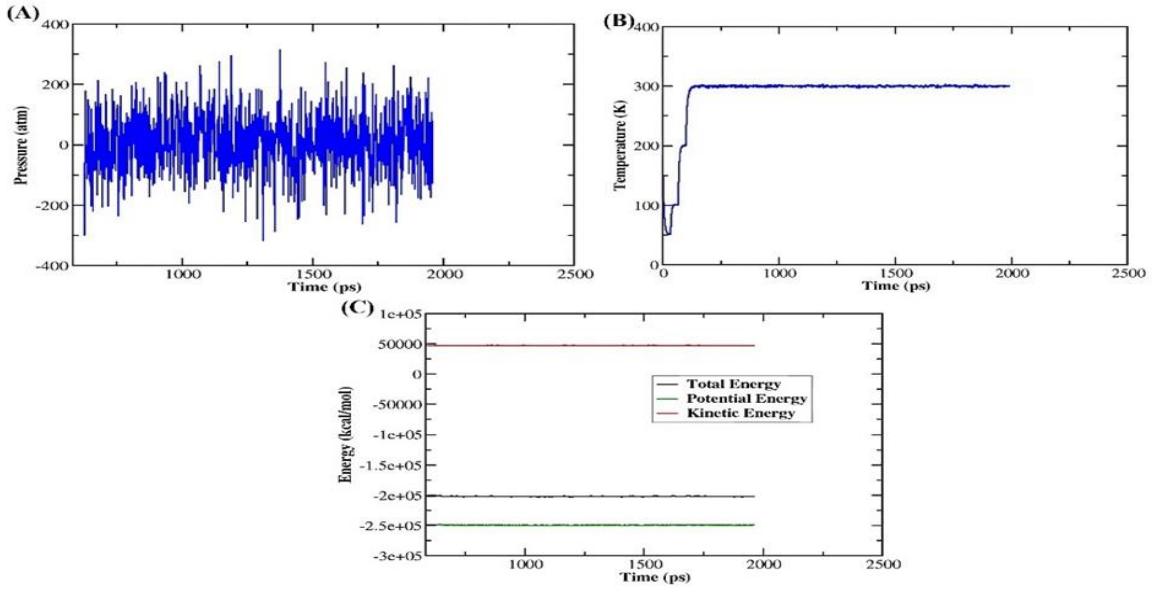

***Figure 6.1**. (A) Pressure (B) Temperature and (C) Energy plots of A30G α-Syn as a function of simulation time*

6.3.3. Prediction of Stability and functioning of α-Synuclein protein upon A30G mutation:

The effect of single point mutation on the stability and functioning of the WT α-Syn was predicted using online servers such as I-Mutant 2.0 [275], CUPSAT [276], MuPro [277], Dynamut [278], Auto-mute [279], Site directed mutator [280], Prem PS [281], SIFT [282], PONDR VLXT [283] and ExPASy ProtParam online tool [284].

I-Mutant is a support vector machine based tool for predicting protein stability changes resulting from single point mutations. CUPSAT predicts protein stability changes in terms of the unfolding free energy difference (ΔΔG) after point mutations using structural environment-specific atom potentials and torsion angle potentials between WT and mutant proteins. Mupro predicts protein stability changes without tertiary structure knowledge. DynaMut is a web application that employs two normal mode approaches, sample conformations and evaluate protein dynamics and stability due to vibrational entropy changes. Auto-mute web-based programmes estimate stability changes after single residue substitutions in proteins with known native structures using cutting-edge supervised classification and regression methods. The SDM is a computational technique that analyses the variation of amino acid replacements occurring at specific structural environments that are tolerated within the family of homologous proteins of known 3-D structures and transforms them into substitution probability tables. These tables are used as a quantitative measurement to forecast protein stability following mutation. PremPS predicts the effects of single-point mutations on protein stability using evolutionary and structure-based features and a symmetrical dataset of stabilising and destabilising mutations. While the SIFT predicts the effects on the protein functioning for a single point mutation that are analysed based on its tolerance/intolerance score.

6.3.4. Construction of Membrane bound α-Synuclein for Molecular Dynamics simulation:

The MD simulations initiated with the 3-D structure of A30G α-Syn, which was built from the WT structure by replacing Alanine with Glycine at position 30 with the UCSF CHIMERA software as shown in **Figure 6.2**. Using the CHARMM GUI, the initial orientation of the protein with respect to the lipid/water interface was predicted using the PPM server [220] as performed in section **4.3.1.** The rest of the MD simulation setup were performed as mentioned in section **4.3.2.**

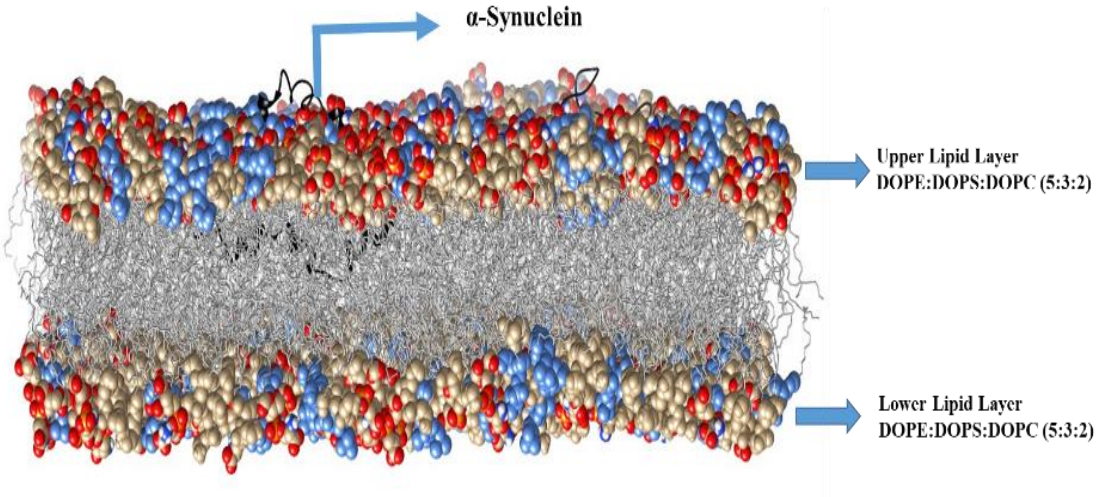

***Figure 6.2**. Graphical illustration of membrane bound A30G α-Syn built using CHARMM GUI server. For better visuals, ions and water box was not included. The snapshots are generated using UCSF CHIMERA 1.14*

6.3.5. Analysis of MD simulation trajectories:

Initially to determine the stabilisation of our complex system, lipid bilayer parameters such as area per lipid, EDP and membrane thickness were investigated. The electron density profile offers a time averaged assessment of the electron density across the lipid bilayer. Area per lipid is the average surface area occupied by a single phospholipid at an interface [458]. The conformational dynamics and other salient structural features of A30G α-Syn as a free monomer in solution and when it is in membrane bound state as a function of time were investigated from the corresponding 100 ns MD trajectory files. The following analysis: RMSD, RMSF, Rg, helical content analysis, Hydrogen bond analysis, secondary structural analysis, inter molecular hydrogen bond analysis, intra molecular hydrogen bond analysis, distance between N-terminal and C-terminal analysis, helical bend analysis, and torsion angle analysis were carried out using cpptraj module [305] of AMBER software package and xmgrace plotting tool was used for generating the plots. PDBsum server [252] was used to get the standard secondary structural components and topology present in the equilibrated structures of the protein.

6.4. Results and Discussions:

In order to confirm if the simulation protocol used is appropriate for the membrane-protein system, a few parameters including APL, membrane thickness and electron density profile, were determined.

6.4.1. Area per lipid analysis of membrane bound A30G α-Synuclein:

The area per lipid analysis determines the compactness of the biomembrane. To find the equilibrium configurations of the DOPE/DOPS/DOPC simulation system, we used the average area per lipid as a parameter. The area per lipid layer value was derived by dividing the lateral surface area of the simulation box by the number of lipids in a leaflet. The time evolution of the APL for the mixed DOPE/DOPS/DOPC lipid bilayer is shown in **Figure 6.3(A)**. The area per lipid analysis in the system was observed to gain acceleration over the first 40 ns before attaining a constant value. For the DOPE/DOPS/DOPC system, the averaged area per lipid over a 100 ns trajectory was determined to be 67.14 $Å^2$ and 69.72 $Å^2$ for the upper leaflet and lower leaflet of lipid, respectively. Additionally, we calculated the average membrane thickness as the shortest distance between a phosphorus atom in one leaflet of a lipid layer and every phosphorus atom in the other leaflet of the lipid layer [459, 460, 300]. The graph in **Figure 6.3(A)** displays the area per lipid of membrane-bound A30G α-Syn, which is relatively steady along the simulation time. The thickness of membrane was averaged over each membrane thickness that each leaflet of individual lipids defined. Membrane thickness plot as observed in **Figure 6.3(B)** displays the time evolution of the membrane thickness for DOPE/DOPS/DOPC mixed lipid bilayers, which are stable during the simulation time period of 100 ns. The average membrane thickness value of the system was calculated to be 78.25 ± 1.707 Å from the trajectory analysis. The average APL value for lipid bilayer (DOPE/DOPS/DOPC) from area per lipid analysis was calculated to be 68.43 $Å^2$, which was close to the experimental average of 65.32 $Å^2$ to 66.32 $Å^2$ [300, 461]. It is observed in **Figure 6.3** that the values of APL and membrane thickness were generally anti-correlated; this relationship might be understood by considering that when the lipid bilayer lateral area is contracted, its head groups are pushed toward the water phase, resulting in a greater membrane thickness that leads to a free energy shift in the position of the membrane interface with water.

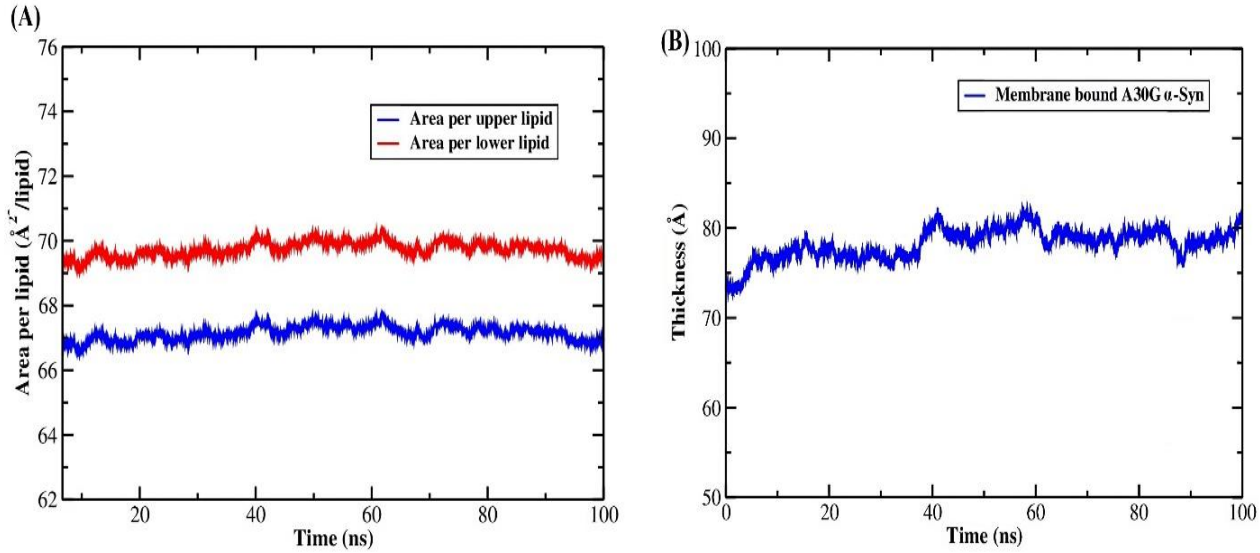

Figure 6.3. *(A) Area per lipid (upper and lower) layer analysis for membrane bound A30G α-Syn during simulation time period of 100 ns (B) the average membrane thickness in angstroms plotted with respect to simulation time period of 100 ns*

6.4.2. Electron Density Profile of lipid membrane bound A30G α-Synuclein:

The EDP were calculated by assuming an electron charge equal to the atomic number minus the atomic partial charge located at the center of each atom. The electron density profile decomposed into various groups such as water, choline (CHOL), phosphate (PO_4), serine, ethanolamine, and oleoyl groups, as plotted in **Figure 6.4(A)**. The density profiles of DOPE, DOPS, and DOPC show that three distinct regions are visible in the case of all atom densities. The mixed lipid bilayer of DOPE, DOPS, and DOPC was characterized by the assembly of a 5:3:2 ratio of the lipids on both lipid monolayers. The EDP for the molecular constituents of the membrane bound A30G α-Syn system were represented in **Figure 6.4(A)**. We found that the electron density was constant on both sides of the membrane at a distance of ±20 Å for all simulated trajectories, indicating that the simulations were well balanced. EDP are commonly used to describe the location of molecules and their chemical components within a bilayer. EDP of different regions in A30G α-Syn have been depicted in **Figure 6.4(B)**. The N-helix region of A30G α-Syn was found to be submerged just under the lipid head group/water interface, enabling the hydrophobic face of the protein to interact with the lipid hydrophobic core and the hydrophilic face to interact with the lipid polar area and water. Despite starting at the same depth, Helix-N ends up at a higher depth beneath the lipid head group phosphates than in the turn region. The helix-C region buries an average of 6 Å below the bilayer center (Z=0). Due to these structural changes, the binding environment of the A30G α-Syn in the

bilayer was drastically altered. Thus, the protein seems to tunnel through the bilayer at times, exposing parts of itself to the water.

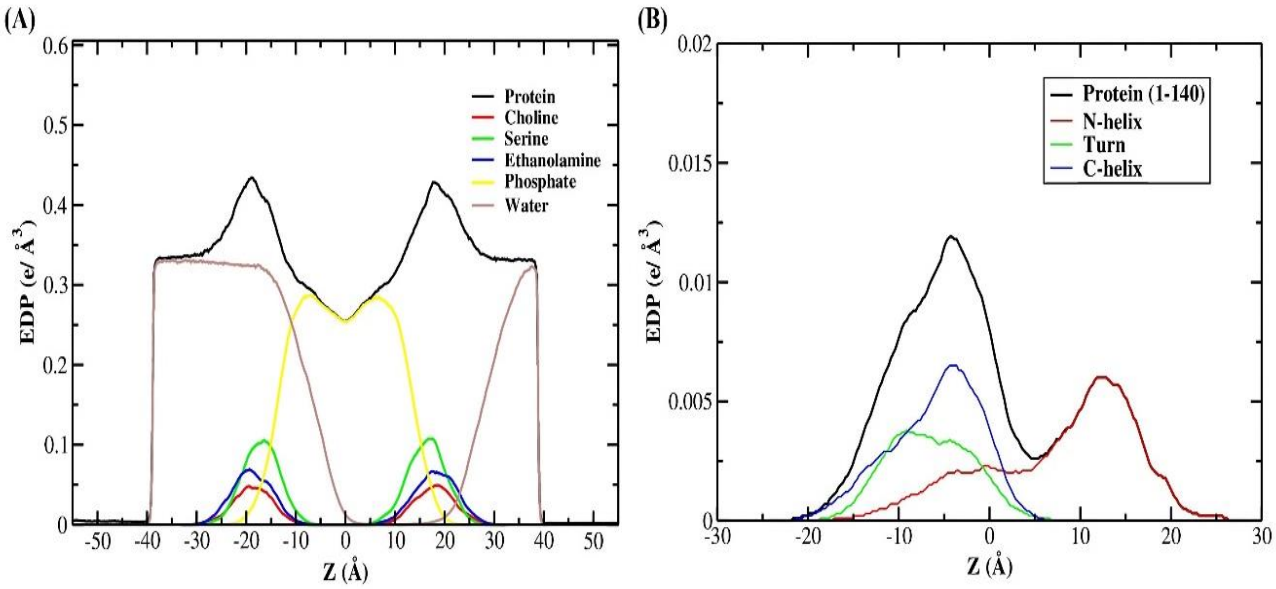

Figure 6.4. *Electron Density Profile (A) of the membrane bound A30G α-Syn and (B) each component of A30G α-Syn*

To compare the conformational properties of (i) A30G α-Syn as a free monomer in solution and (ii) when bound to a lipid membrane, we have carried out corresponding MD simulation trajectory analysis.

6.4.3. Snapshots of A30G α-Synuclein in free monomer form and when bound to membrane bilayer:

The snapshots of A30G α-Syn in membrane bound state and in free solution were obtained from the corresponding 100 ns MD trajectories as shown in **Figure 6.5 and 6.6** respectively. From **Figure 6.5**, the major portion of membrane bound A30G α-Syn was seen to be embedded into the hydrophobic core of the lipid bilayer, beneath the lipid head group, forming channels. In particular, the N-helix is submerged beneath the lipid membrane, followed by the NAC and the C-helix, as shown in **Figure 6.5**. Throughout the simulation time period, the helices are securely immersed in these channels despite a significant degree of variability. A30G α-Syn structure in free monomer form (**Figure 6.6**) is destabilized due to decrease in secondary helical structural content. From the snapshots in **Figure 6.6**, we observed that the secondary structure in the N-terminal and NAC region of A30G α-Syn changes rapidly in the free monomer form. Membrane bound A30G α-Syn has abundant basic side chains and acidic side chains that point along the bilayer surface and the solvent respectively while the nonpolar side chains point

toward the bilayer center **(Figure 6.7**). It is reported [432] that N-terminal region of α-Syn found to contain seven imperfect copies of an 11-mer repeat and most of this repeat observed to contain two (i, i+2) lysine residues. In the case of membrane bound A30G α-Syn as shown in **Figure 6.8**, we observed these paired lysine side chains point in opposite directions along the lipid bilayer surface and having impact on helical depth and topology. The highly hydrophobic sixth 11-mer repeat present within the largely hydrophobic NAC region (61-95) found to place deep into lipid bilayer and this particular region has been highlighted to drive fibril formation [138,462]. In membrane bound A30G α-Syn, Helix-C was observed to be elevated from the lipid bilayer surface while helix-N and turn are submerged into the lipid bilayer surface. The N-terminal region in membrane-bound A30G α-Syn was found to act as an anchor to the lipid membrane and was believed to play a significant role in retaining the conformation while the C-terminal region was found to be unbound and forming lesser interaction with the lipid membrane. The C-terminal region has been reported earlier to remain unbound and available for potential interactions with other proteins [463]. Different regions of α-Syn displayed distinct interaction modalities rather than binding uniformly to membranes as a single entity, and other investigations reported comparable outcomes [18, 226].

(A)

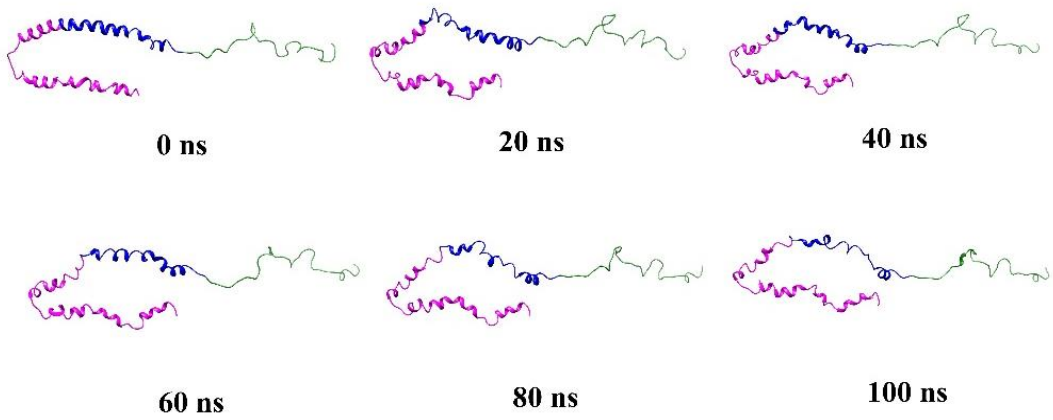

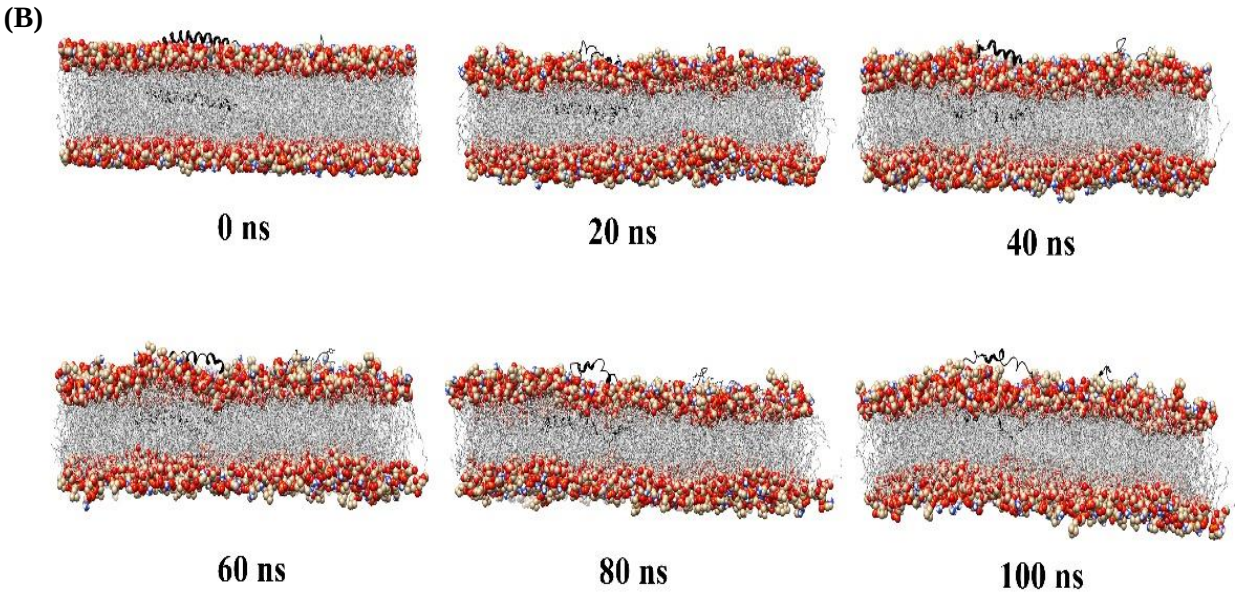

***Figure 6.5**. Snapshots of (A) membrane bound A30G α-Syn and (B) membrane bound (hidden) A30G α-Syn after simulation time period of 100 ns*

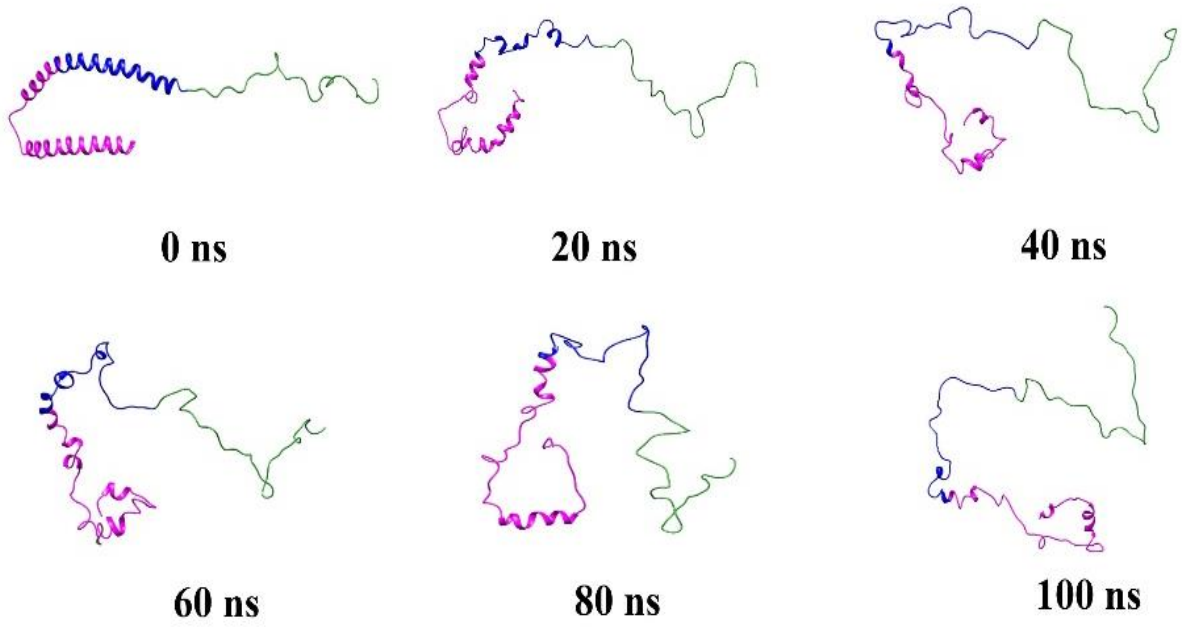

***Figure 6.6**. Snapshots of A30G α-Syn as a monomer in free solution after simulation time period of 100 ns. A30G α-Syn backbone is represented as N-helix (pink), turn (blue) and C-helix (green)*

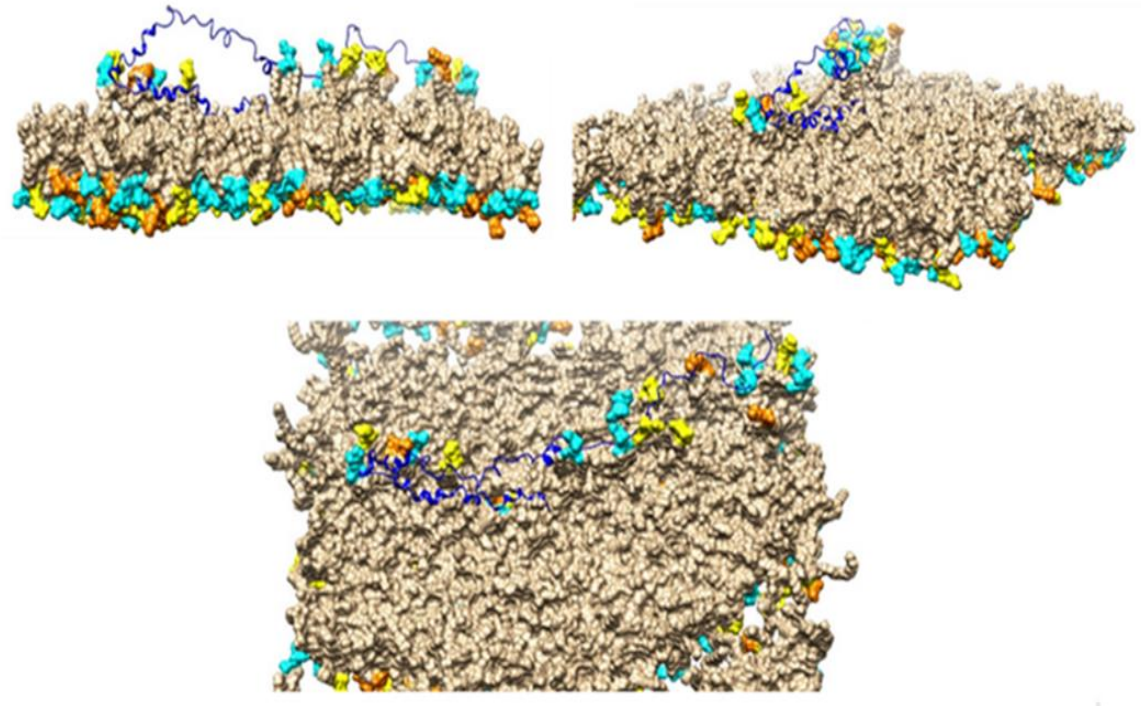

Figure 6.7. *Snapshots of A30G α-Syn conformations on its interaction with the lipid membrane after 100 ns of simulated dynamics*

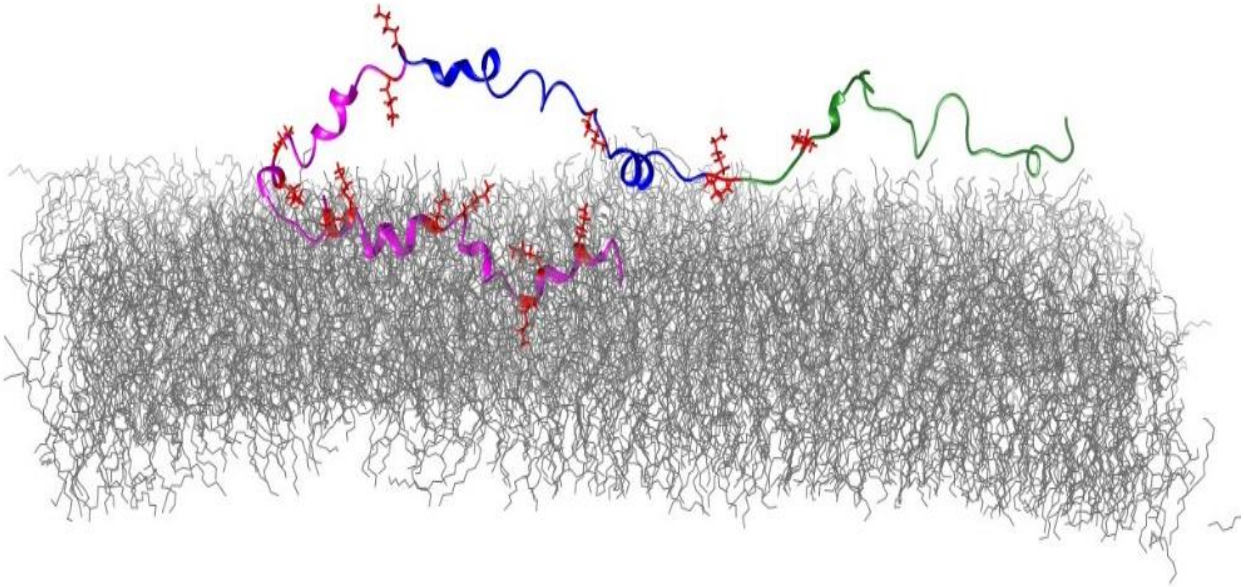

Figure 6.8. *Snapshot of membrane bound A30G α-Syn showing two (i, i+2) paired lysine residues in opposite direction along the lipid bilayer surface*

6.4.4. RMSD Analysis:

The MD analysis of the Cα RMSD of the three regions (N-terminal, NAC and C-terminal) of membrane-bound A30G α-Syn and free monomer have been depicted in **Figure 6.9(A) and 6.9(B)** respectively. Similarly, the Cα RMSD of the entire A30G α-Syn protein in free form and membrane bound form has been depicted in **Figure 6.9(C)**. There is a subtle difference in the Cα RMSD values of the three regions of A30G because these regions interact distinctly with the membrane and not as a single entity throughout the simulation time. The A30G α-Syn protein was found to show rapid change in the conformation when it is in the free form than in the membrane bound form. In free solution **(Figure 6.9(B))**, it was found that the RMSD values of the three regions of A30G α-Syn fluctuated considerably and had poor convergence. This is due to the lack of proper force field parameters for analysing the MD of IDP, which are characterised by rapid flexibility and dynamics with high amplitude, as well as the fact that limited aqueous volume effects were not taken into account in MD simulations of IDP in water [464-466].

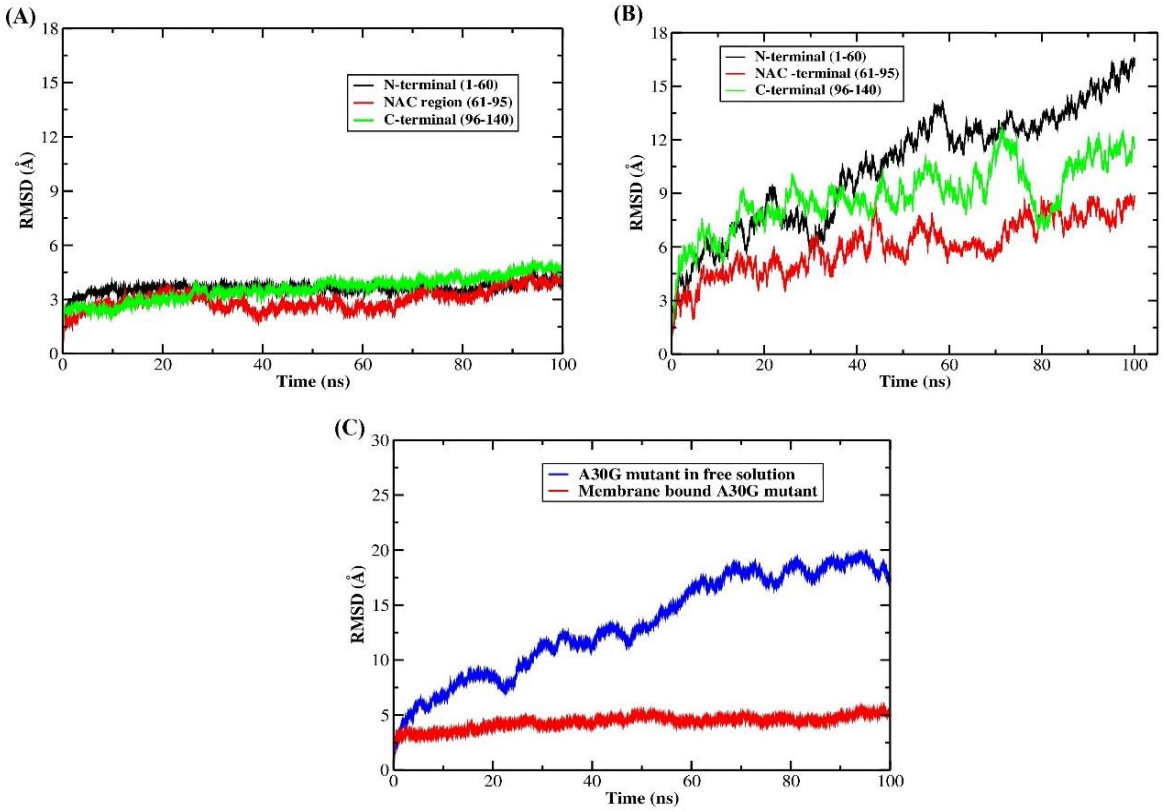

Figure 6.9. *RMSD analysis of N-terminal, NAC region and C-terminal of (A) membrane bound A30G α-Syn (B) A30G α-Syn in free solution. (C) Comparison of Cα RMSD for membrane bound A30G α-Syn and in free solution during MD simulation of 100 ns*

6.4.5. Radius of gyration Analysis:

The Rg is typically calculated to determine the dispersion of atoms in a given biomolecule from their common axis or centre of gravity. The compactness of a protein structure can be determined using Rg [406]. The distribution of Rg values of the A30G α-Syn in membrane bound and free form as a function of simulation time have been depicted in **Figure 6.10**. From the Rg plot, we see that the Rg value for the A30G α-Syn in free form was in the range 47- 49 Å, while in the membrane bound form the value drops to around 33 Å. From the Rg analysis, we can infer that the structure of A30G α-Syn was more compact in the case of membrane bound form than in the free form. Moreover, the observed changes in Rg values reflect the diverse conformations of the A30G α-Syn structure and their molecular interactions over the duration of the simulation time.

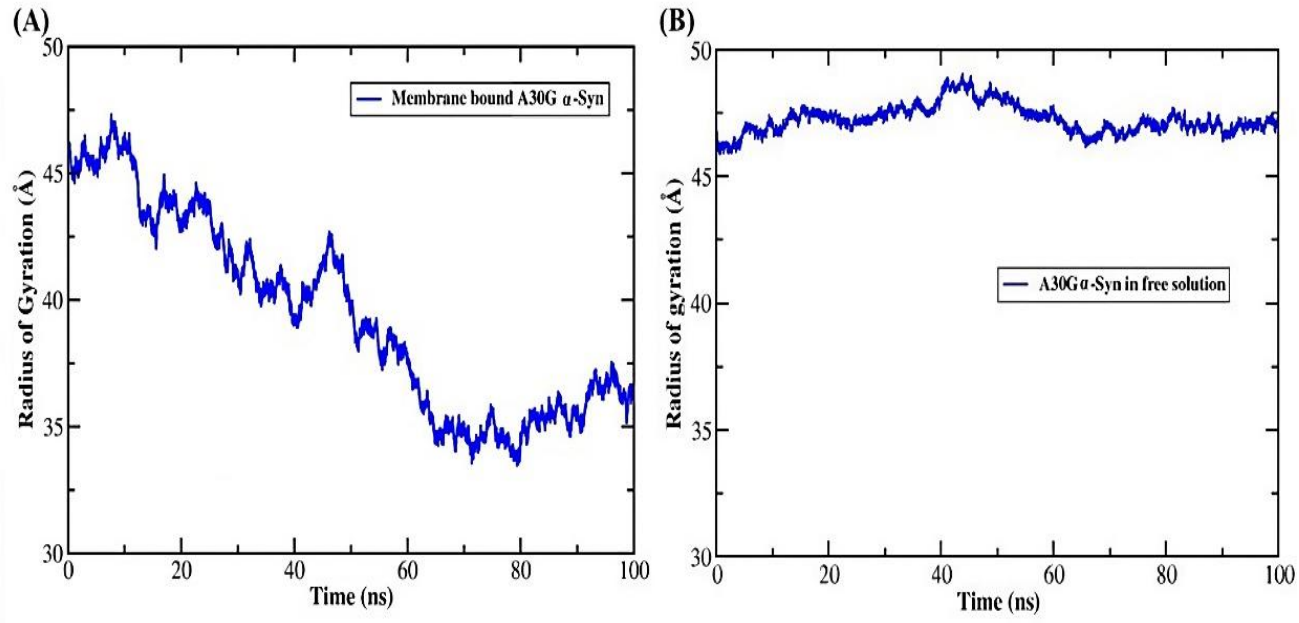

***Figure 6.10**. Radius of gyration analysis of (A) membrane bound state A30G α-Syn and (B). A30G α-Syn in free solution during simulation time*

6.4.6. RMSF Analysis:

The RMSF plots demonstrate the flexibility of individual residues during the simulation time period. The RMSF data for A30G α-Syn in membrane bound state and in free solution were depicted in **Figure 6.11(A) and 6.11(B)** respectively. There is an increase in flexibility close to the site of the mutation since glycine residue is known to promote flexibility in the backbone and often favours turn while alanine residue typically favours helix. Also, the

protein dynamics (flexibility) was noticed to get lowered in the N-terminal region in the case of α-Syn when it is in membrane bound form.

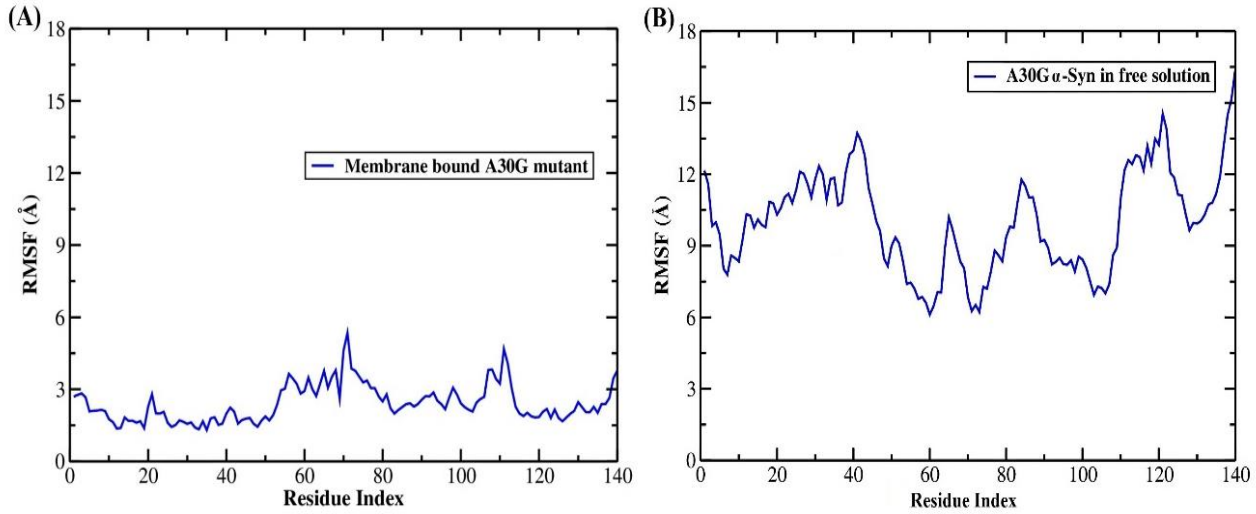

Figure 6.11. *RMSF analysis of (A) membrane bound A30G α-Syn and (B) A30G α-Syn in free monomeric form in solution during simulation time period of 100 ns*

6.4.7. Secondary Structural Analysis:

To calculate secondary structural propensities for all the residues in A30G α-Syn protein in the free monomer form and membrane bound state, the DSSP method of Kabsch and Sander was used, which assigns secondary structure types for residues based on backbone amide (N-H) and carbonyl (C=O) atom positions (**Figure 6.12 and Figure 6.13**). In comparison with A30G α-Syn in free solution, membrane bound A30G α-Syn was found to contain relatively higher helicity in N-helix (3-37) and turn region (38-44). Further in the membrane bound form of A30G α-Syn, the helicity was observed to get disrupted in those regions that are elevated above the surface of lipid bilayer. Similar secondary structure profile has been reported in the earlier study on A30G α-Syn [155], indicating decrease in the alpha helical propensity. The surface topology for the equilibrated structure of A30G α-Syn protein in the free monomer form and membrane bound state obtained from PDBsum server [252] were shown in **Figure 6.14**. The number of helices were observed to be higher in A30G α-Syn when it is associated with membrane. The helices (along with the residue index, length and sequence) noticed in surface topology of the structure of A30G α-Syn protein in the membrane bound and free form have been depicted in **Figure 6.15** and **Figure 6.16** respectively.

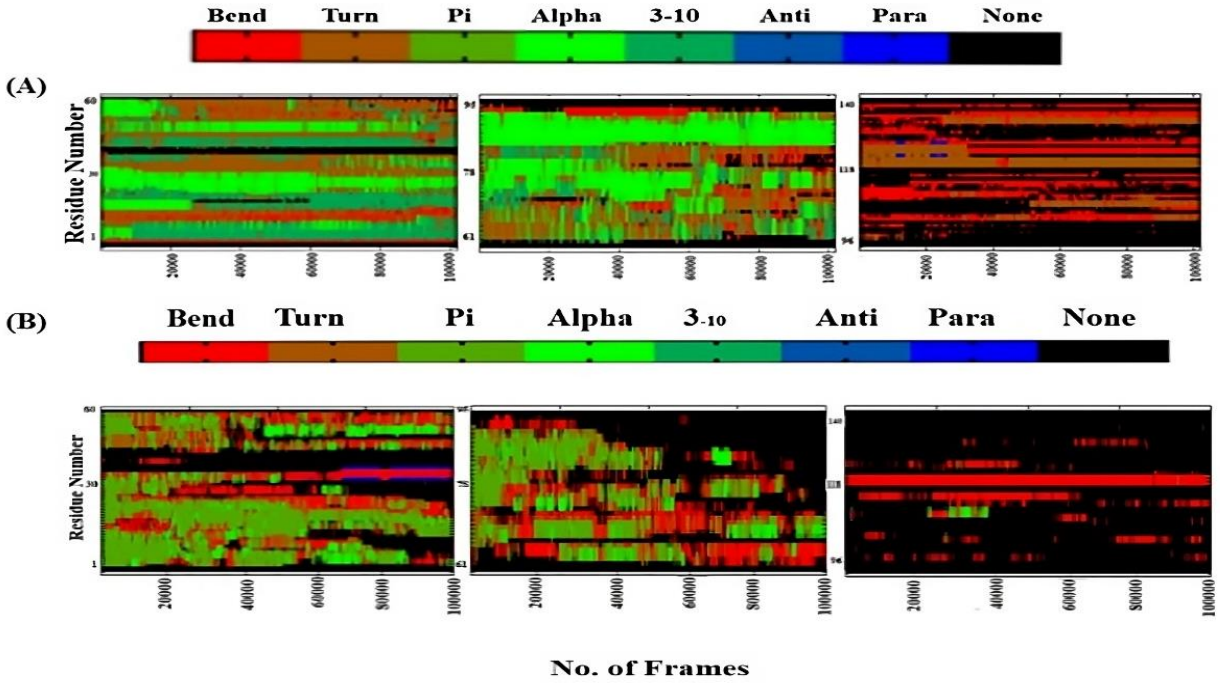

Figure 6.12. *Secondary structural analysis of (A) A30G α-Syn in membrane bound form (B) A30G α-Syn in free monomer form*

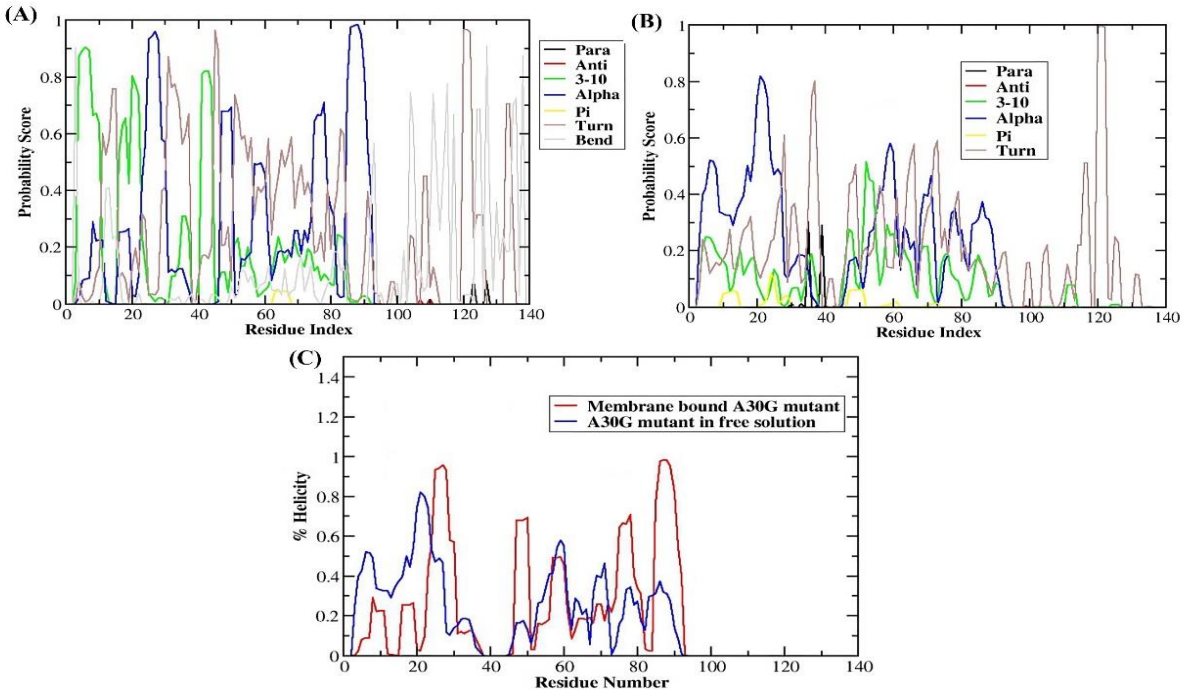

Figure 6.13. *Secondary structure Probability score of (A) membrane bound A30G α-Syn and (B) A30G α-Syn in free monomer form*

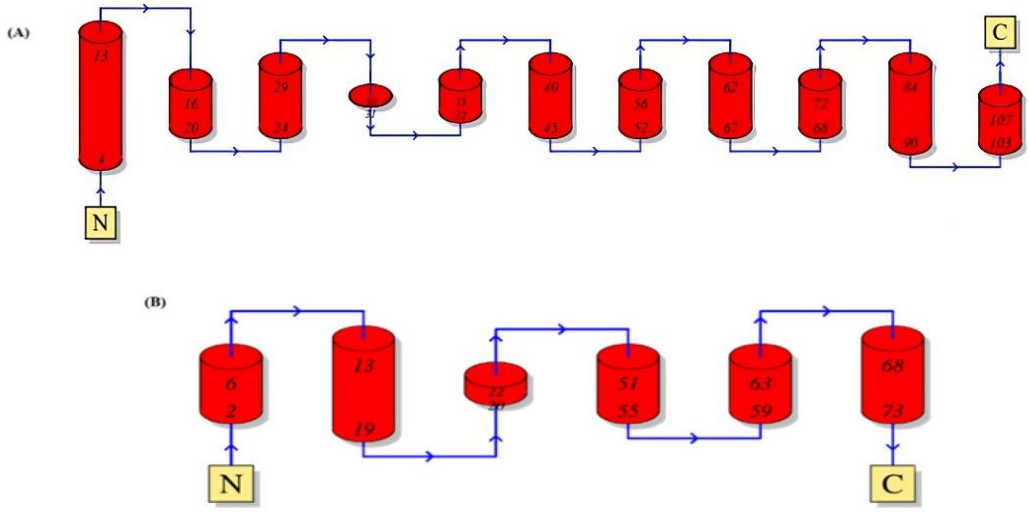

Figure 6.14. *Surface topology analysis of (A) membrane bound A30G α-Syn and (B) A30G α-Syn in free monomer form during the simulation time*

Helix 1. Met5-Lys12
Sequence: MKGLSKAK
Length: 8 residues

Helix 2. Ala17-Ala19
Sequence: AAA
Length: 3 residues

Helix 3. Gly25-Glu28
Sequence: GVAE
Length: 4 residues

Helix 4. Lys32-Lys34
Sequence: KTK
Length: 3 residues

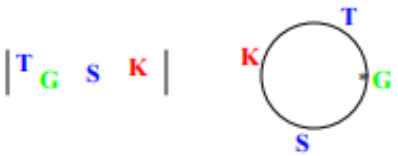

Helix 5. Gly41-Thr44
Sequence: GSKT
Length: 4 residues

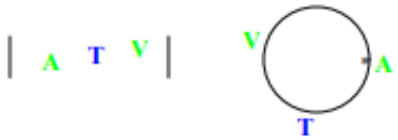

Helix 6. Ala53-Val55
Sequence: ATV
Length: 3 residues

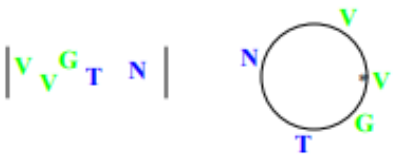

Helix 7. Val63-Gly67
Sequence: VTNVG
Length: 5 residues

Helix 8. Gly68-Val71
Sequence: GAVV
Length: 4 residues

Helix 9. Ala85-Ala89
Sequence: AGS I A
Length: 5 residues

Helix 10. Glu104-Gly106
Sequence: E E G
Length: 3 residues

Figure 6.15. *List of helices observed in membrane bound A30G α-Syn during the simulation time*

Helix 1. Val3-Met5
Sequence: V F M
Length: 3 residues

Helix 2. Gly14-Ala18
Sequence: G V V A A
Length: 5 residues

Helix 3. Ala19-Lys21
Sequence: A E K
Length: 3 residues

Helix 4. Val52-Thr54
Sequence: V A T
Length: 3 residues

Helix 5. Lys60-Gln62
Sequence: K E Q
Length: 3 residues

Helix 6. Ala69-Thr72
Sequence: A V V T
Length: 4 residues

Figure 6.16. *List of helices observed in A30G α-Syn in free solution during the simulation time*

6.4.8. Intermolecular Hydrogen bond Analysis:

The number of intermolecular hydrogen bonds between the lipid bilayer and A30G α-Syn as a function of simulation time was shown in **Figure 6.17**. The average number of intermolecular hydrogen bonds between the A30G α-Syn and the lipid bilayer was

calculated to be 20. The atomic level details regarding the intermolecular hydrogen bonds between lipid bilayer (acceptor/donor) and A30G α-Syn (acceptor/donor) were summarized in **Table 6.1 and Table 6.2** respectively. The number of inter-molecular hydrogen bonds between different regions (N-terminal, NAC and C-terminal) of A30G α-Syn and the lipid bilayer as a function of simulation time were depicted in **Figure 6.18**. From **Figure 6.18**, it is apparent that N-terminal region of A30G α-Syn to have higher number of intermolecular hydrogen bonds with the lipid bilayer. This suggests that instead of attaching evenly to membranes as a single entity, the different regions of α-Syn exhibit discrete interaction modes. A study on the phospholipid binding modes of α-Syn has previously shown similar results [18, 226].

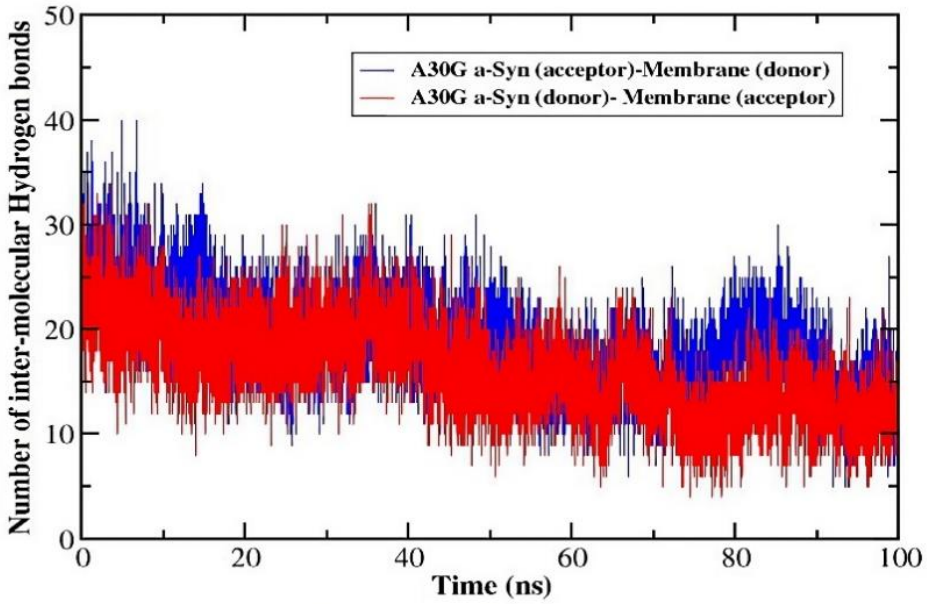

Figure 6.17. *The number of intermolecular hydrogen bonds between N-terminal, NAC region and C-terminal of membrane bound A30G α-Syn during MD simulation of 100 ns*

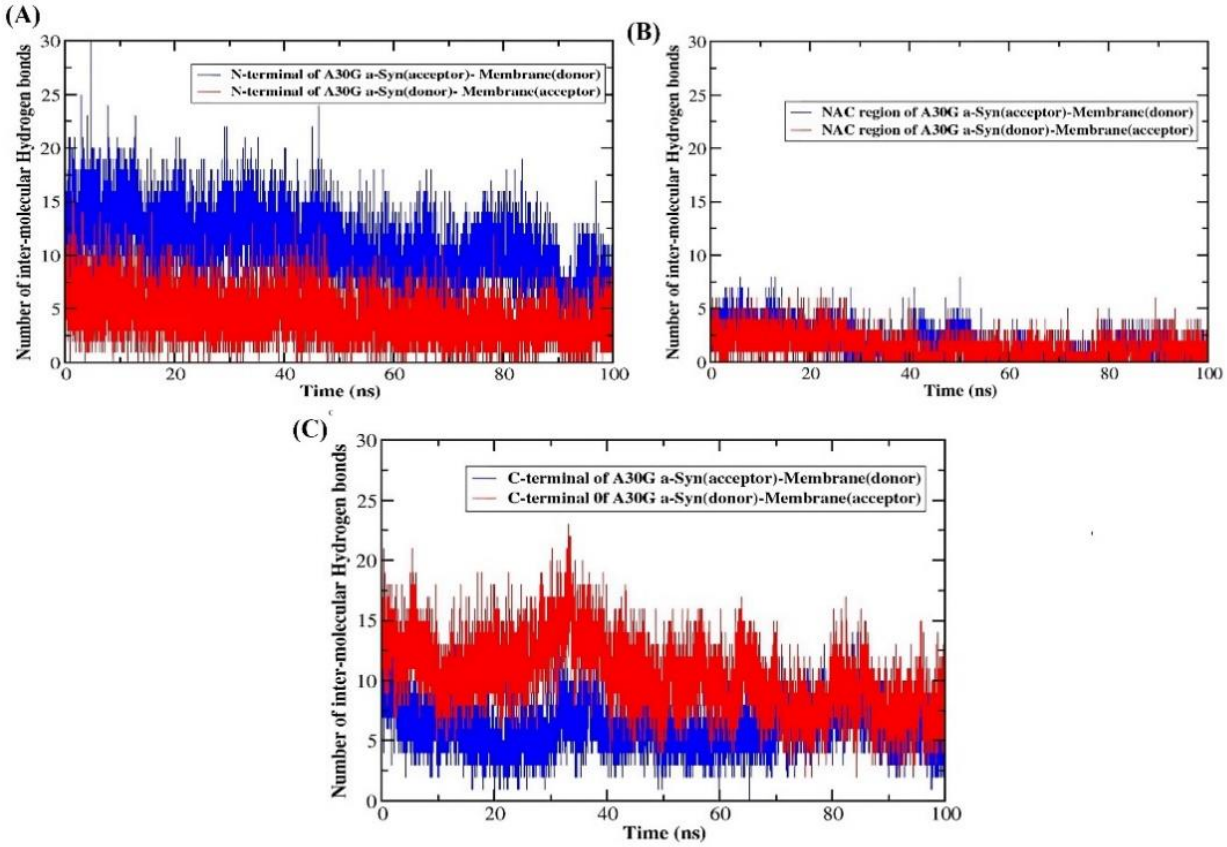

Figure 6.18. *The number of intermolecular hydrogen bonds between membrane bilayer and (A) N-terminal, (B) NAC region and (C) C-terminal of A30G α-Syn during MD simulation of 100 ns*

Table 6.1. *Intermolecular Hydrogen bond analysis of membrane bound A30G mutant complex during the MD simulation of 100 ns with membrane bilayer as acceptor and A30G mutant as donor*

#Acceptor	DonorH	Donor	Average Distance (Å)	Average Angle (º)
PE_1897@O34	SER_129@HG	SER_129@OG	2.6285	165.6359
PE_1801@O22	GLY_41@H	GLY_41@N	2.8446	159.98
PE_1810@O12	SER_129@H	SER_129@N	2.8495	158.5444
PC_1807@O33	LYS_43@HZ1	LYS_43@NZ	2.7722	162.3433
PC_1825@O34	THR_54@HG1	THR_54@OG1	2.6838	164.4802
PE_1777@O12	TYR_133@HH	TYR_133@OH	2.6859	164.191
PE_1903@O22	LYS_97@HZ3	LYS_97@NZ	2.7517	156.762
PC_1825@O34	LYS_58@HZ1	LYS_58@NZ	2.727	159.7241
PS_1864@O33	LYS_21@HZ3	LYS_21@NZ	2.7371	156.199
PC_1843@O34	LYS_21@HZ2	LYS_21@NZ	2.761	158.159
PE_1903@O34	LYS_97@HZ2	LYS_97@NZ	2.7664	155.952
PE_1813@O22	SER_87@HG	SER_87@OG	2.6582	162.6684
PC_1855@O34	LYS_58@HZ1	LYS_58@NZ	2.7677	157.1248
PE_1903@O22	LYS_97@HZ1	LYS_97@NZ	2.7619	155.1759

PE_1903@O34	LYS_97@HZ3	LYS_97@NZ	2.7667	156.2453
PE_1903@O22	LYS_97@HZ2	LYS_97@NZ	2.7523	154.908
PE_1882@O34	GLU_110@H	GLU_110@N	2.833	160.0708
PS_1819@O36	GLY_93@H	GLY_93@N	2.8214	160.9648
PE_1813@O34	LYS_80@HZ2	LYS_80@NZ	2.7195	160.0082
PE_1903@O34	LYS_97@HZ1	LYS_97@NZ	2.7659	156.4536
PE_145@O34	LYS_12@HZ3	LYS_12@NZ	2.7346	157.5749
PC_1825@O34	LYS_58@HZ2	LYS_58@NZ	2.7234	158.9376
PS_1864@O33	LYS_21@HZ2	LYS_21@NZ	2.754	157.6096
PE_1813@O34	LYS_80@HZ3	LYS_80@NZ	2.7493	158.3565
PE_1837@O34	LYS_102@HZ3	LYS_102@NZ	2.7633	158.7418
PS_1849@O22	LYS_32@HZ3	LYS_32@NZ	2.7869	153.3245
PE_1840@O22	LYS_102@HZ3	LYS_102@NZ	2.7817	158.6006
PC_1825@O22	GLN_24@HE22	GLN_24@NE2	2.8405	158.327
PE_1795@O12	ASP_98@H	ASP_98@N	2.8287	153.3121
PC_1807@O33	LYS_43@HZ2	LYS_43@NZ	2.7744	159.777
PS_1849@O22	LYS_32@HZ1	LYS_32@NZ	2.7742	153.7054
PS_1969@O35	LYS_58@HZ2	LYS_58@NZ	2.7646	156.5703
PE_145@O12	LYS_12@HZ3	LYS_12@NZ	2.7668	154.1987
PE_145@O12	LYS_12@HZ2	LYS_12@NZ	2.7638	154.1514
PS_1969@O36	LYS_58@HZ3	LYS_58@NZ	2.7919	157.1917
PE_1867@O34	LYS_80@HZ1	LYS_80@NZ	2.7528	158.2396
PE_1867@O34	LYS_80@HZ3	LYS_80@NZ	2.7519	159.1118
PS_1774@O34	LYS_97@HZ1	LYS_97@NZ	2.7512	156.856
PE_145@O34	LYS_12@HZ2	LYS_12@NZ	2.7347	155.471
PC_1861@O22	THR_44@HG1	THR_44@OG1	2.7024	162.7958
PE_1840@O22	LYS_102@HZ2	LYS_102@NZ	2.7829	157.175
PC_1855@O34	LYS_58@HZ3	LYS_58@NZ	2.7742	157.0093
PC_1855@O34	LYS_58@HZ2	LYS_58@NZ	2.7563	157.135
PC_1924@O33	LYS_6@HZ3	LYS_6@NZ	2.7625	161.5987
PC_1807@O34	LYS_43@HZ2	LYS_43@NZ	2.7345	153.8534
PS_1849@O33	LYS_32@HZ1	LYS_32@NZ	2.7369	155.9202
PC_1825@O34	LYS_58@HZ3	LYS_58@NZ	2.716	159.6001
PS_1864@O33	LYS_21@HZ1	LYS_21@NZ	2.7495	157.2289
PS_1828@O34	LYS_45@HZ1	LYS_45@NZ	2.7659	157.9742

Table 6.2. *Intermolecular Hydrogen bond analysis of membrane bound A30G mutant complex during the MD simulation of 100 ns with A30G mutant as acceptor and membrane bilayer as donor*

#Acceptor	DonorH	Donor	Average Distance (Å)	Average Angle (º)
SER_129@O	PE_1810@HN1A	PE_1810@N31	2.811	156.6154
LEU_100@O	PE_1840@HN1A	PE_1840@N31	2.7877	157.1605
LEU_100@O	PE_1840@HN1C	PE_1840@N31	2.7839	155.7935
GLU_105@OE2	PE_1762@HN1A	PE_1762@N31	2.7479	157.9234

SER_129@O	PE_1810@HN1B	PE_1810@N31	2.8114	156.154
ASP_98@OD1	PE_1840@HN1C	PE_1840@N31	2.8045	152.7825
ASP_98@OD1	PE_1840@HN1B	PE_1840@N31	2.8141	152.5015
SER_129@O	PE_1810@HN1C	PE_1810@N31	2.8059	155.26
GLU_105@OE1	PE_1837@HN1C	PE_1837@N31	2.777	158.893
TYR_125@O	PE_1798@HN1A	PE_1798@N31	2.8028	152.5876
GLU_126@OE2	PS_1792@HN1B	PS_1792@N31	2.7909	158.073
GLU_114@O	PS_1873@HN1A	PS_1873@N31	2.8072	154.7328
MET_116@O	PE_1846@HN1A	PE_1846@N31	2.8237	151.5765
GLU_114@O	PS_1873@HN1B	PS_1873@N31	2.8084	155.2796
ASP_115@OD1	PE_1846@HN1C	PE_1846@N31	2.8111	153.5508
GLU_105@OE1	PE_1762@HN1B	PE_1762@N31	2.7943	154.8064
GLU_137@OE1	PE_1777@HN1A	PE_1777@N31	2.7606	154.7792
ASP_115@OD2	PE_1846@HN1C	PE_1846@N31	2.8063	153.166
ASP_98@OD2	PS_1774@HN1B	PS_1774@N31	2.7943	159.204
ALA_76@O	PE_1834@HN1B	PE_1834@N31	2.7948	155.827
MET_116@O	PE_1846@HN1B	PE_1846@N31	2.8148	152.6343
GLU_105@OE1	PE_1837@HN1B	PE_1837@N31	2.7684	159.1382
ASP_98@OD2	PE_1840@HN1B	PE_1840@N31	2.81	152.1297
GLU_131@OE1	PS_1858@HN1C	PS_1858@N31	2.7812	157.282
GLU_131@OE2	PS_1858@HN1B	PS_1858@N31	2.7875	154.3126
LEU_100@O	PE_1840@HN1B	PE_1840@N31	2.7906	156.3183
GLU_105@OE1	PE_1762@HN1C	PE_1762@N31	2.7993	157.0799
GLU_105@OE1	PE_1762@HN1A	PE_1762@N31	2.7859	154.8279
GLU_114@O	PS_1873@HN1C	PS_1873@N31	2.8169	154.2518
ASP_115@OD2	PE_1846@HN1B	PE_1846@N31	2.7981	153.5483
GLU_137@O	PE_1777@HN1B	PE_1777@N31	2.838	157.3664
TYR_125@O	PE_1798@HN1B	PE_1798@N31	2.8019	152.7322
GLU_131@OE2	PE_1954@HN1C	PE_1954@N31	2.7945	154.4037
GLU_105@OE2	PE_1762@HN1B	PE_1762@N31	2.7895	153.3099
ASP_98@OD1	PE_1840@HN1A	PE_1840@N31	2.8056	152.3008
ALA_140@O	PE_1876@HN1C	PE_1876@N31	2.7906	154.5879
GLU_131@OE1	PE_1954@HN1A	PE_1954@N31	2.8057	154.3825
THR_92@OG1	PS_1819@HN1B	PS_1819@N31	2.8553	156.3471
GLU_105@OE2	PE_1762@HN1C	PE_1762@N31	2.779	154.1564
ASN_122@O	PE_1798@HN1C	PE_1798@N31	2.801	153.197
MET_116@O	PE_1846@HN1C	PE_1846@N31	2.8189	152.6975
TYR_125@O	PE_1798@HN1C	PE_1798@N31	2.7989	152.6711
ASP_119@OD2	PE_1846@HN1B	PE_1846@N31	2.7823	156.3378
THR_92@OG1	PS_1819@HN1A	PS_1819@N31	2.8594	155.0706
GLU_131@OE1	PE_1810@HN1C	PE_1810@N31	2.7693	157.3662
GLU_131@OE1	PE_1954@HN1C	PE_1954@N31	2.8284	153.6049
ASP_119@OD1	PE_1846@HN1B	PE_1846@N31	2.7861	157.1547
GLU_110@OE1	PE_1882@HN1C	PE_1882@N31	2.7805	157.6344

GLU_105@OE1	PE_1837@HN1A	PE_1837@N31	2.7729	158.526
ASP_115@OD2	PE_1846@HN1A	PE_1846@N31	2.8072	151.5374

6.4.9. Intramolecular Hydrogen bond Analysis:

The number of intra-molecular hydrogen bonds were calculated to investigate the proximity of all atom interactions within the membrane-bound A30G α-Syn and in free solution. Intramolecular hydrogen bond contacts are important determinants of A30G α-Syn structural compactness within the different regions of A30G α-Syn. The results obtained in **Figure 6.19** showed higher intra-molecular contacts within the N-terminal region (1-60) than NAC region (61-95) and C-terminal region (96-140). According to the results observed from the analysis in **Figure 6.19(A)** and **6.19(B)**, the average number of intramolecular hydrogen bonds were found to be higher in the N-terminal region of membrane bound A30G α-Syn than in the free monomer form. There is no significant difference in the number of intramolecular hydrogen bonds present in the NAC and C-terminal regions of A30G α-Syn in membrane bound and free monomer form. But in the N-helix, turn and C-helix regions, the number of intramolecular hydrogen bonds were found to be relatively higher in the A30G α-Syn in membrane bound form than in the free monomeric form in solution (as shown in **Figure 6.19(C)** and **Figure 6.19(D)**). In membrane bound A30G α-Syn, the N-helix and turn are deeply buried beneath the lipid bilayer surface.

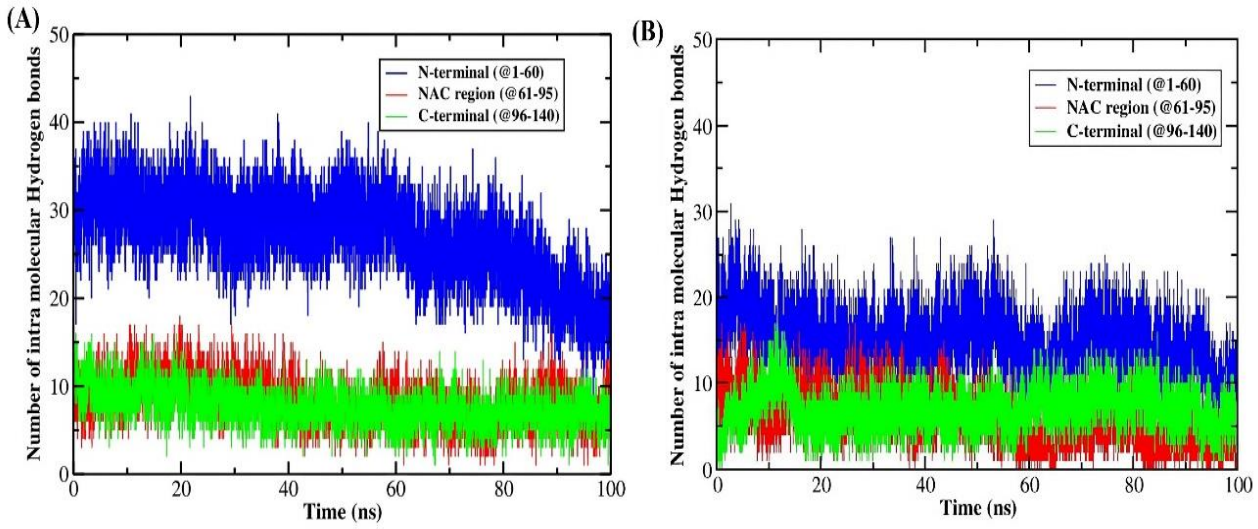

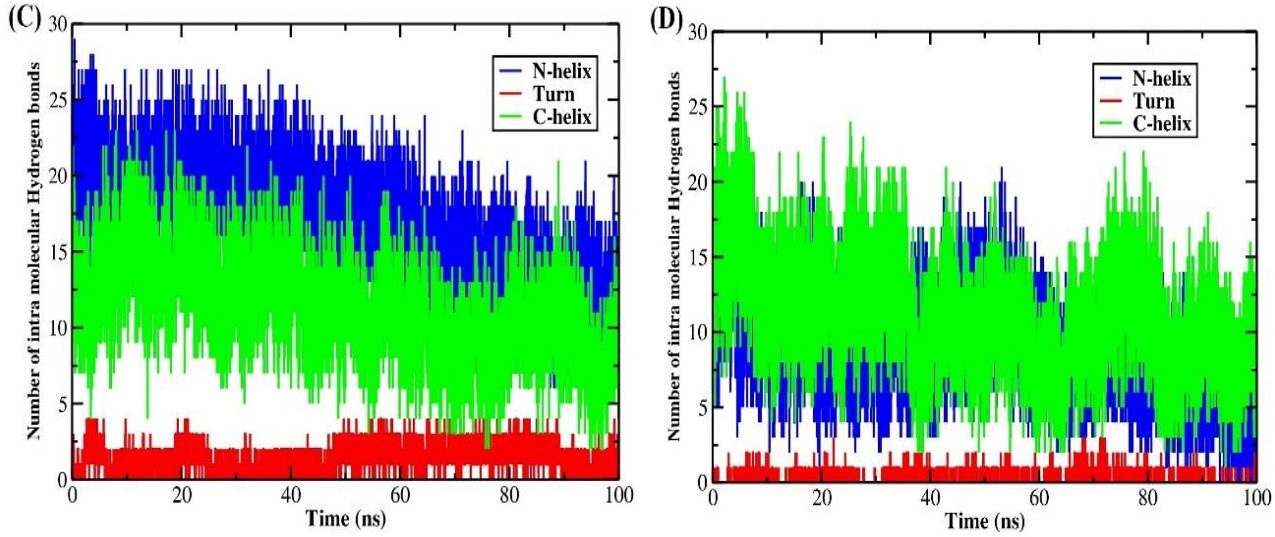

Figure 6.19. *The number of intramolecular hydrogen bonds within N-terminal, NAC region and C terminal of (A) A30G α-Syn in membrane bound form and (B) in free form during MD simulation time. The number of intramolecular hydrogen bonds within N-helix, Turn and C-helix of (C) A30G α-Syn in membrane bound form and (D) in free form during MD simulation time*

6.4.10. Analysis of distance between N-terminal and C-terminal regions:

The centre of mass distance between the N-terminal and C-terminal region of A30G α-Syn in membrane bound form and in free form were analysed as a function of simulation time **Figure 6.20**. The distance between N-terminal and C-terminal was found to be lower in free monomer form of A30G α-Syn than in the membrane bound state. This is because in the membrane bound form, the N-terminal region is buried deeply into the lipid bilayer. In contrast, in the free monomer form, it was discovered that the helical structure in the N-terminal region is more severely broken and coils, which significantly reduces the distance between the N-terminal and C-terminal.

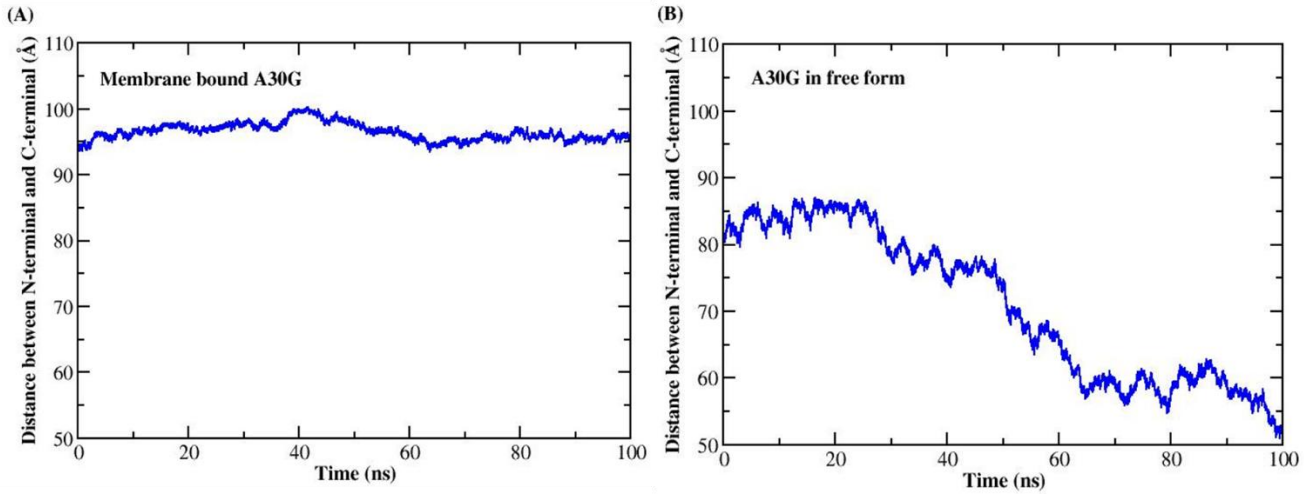

Figure 6.20. *Distance analysis between N-terminal and C-terminal domains of (A) membrane bound A30G α-Syn and (B) A30G α-Syn as a free monomer in solution*

6.4.11. Helical bend Analysis:

The helical bending mechanism, which is a subset of all the dynamic simulations, is of particular interest. The typical equilibrium conditions that can both be reflected by bending are a) equilibrium fluctuations that firmly connects the form of the helices to that of the lipid bilayer, and b) impact of mutation on the interaction between protein and the lipid bilayer. The helical bending at each residue was determined as the angle between the two helical axes formed by the four upstream and downstream residues. The membrane bound form of A30G α-Syn and the free form shows a minimum bending of α-helix equilibrated at an angle of 37^0 and 38.5^0 respectively as shown in **Figure 6.21(A) and 6.21(B)**.

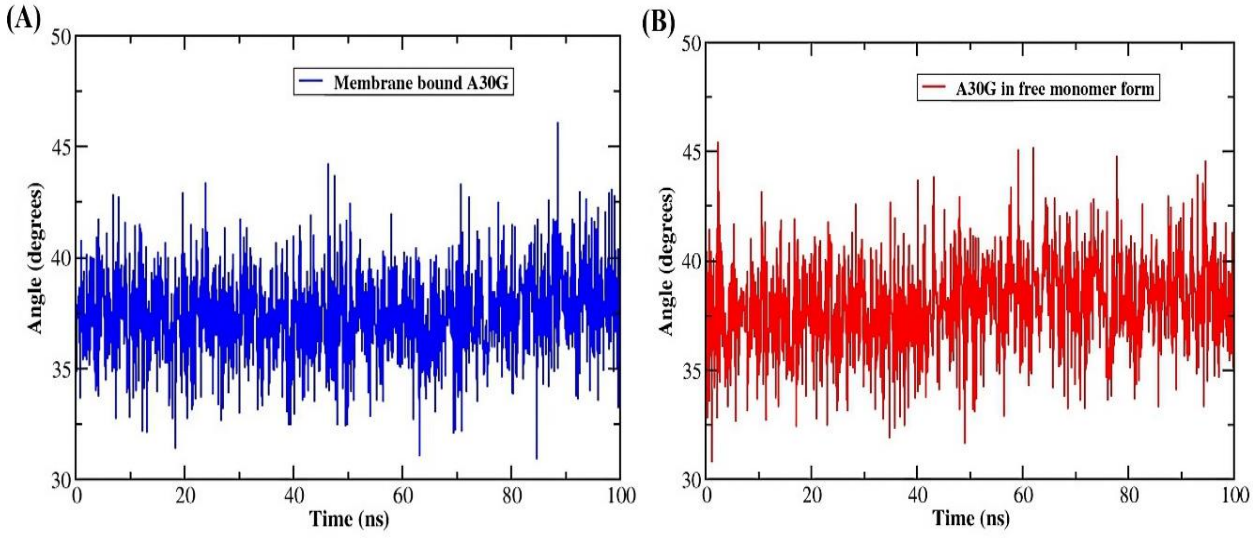

***Figure 6.21**. Helical bending at position Glycine 67/68 during the simulation period of 100 ns. The color scheme is as follows: (A) A30G α-Syn in lipid-bound state (blue) and (B) free monomer state (red)*

6.4.12. Torsion angle analysis:

The time evolution of backbone torsion angles is another technique to illustrate the dynamic conformational shifts of the A30G α-Syn in free monomer state and in membrane bound state. The A30G α-Syn in free monomer form showed significant deviation from its typical α-helical torsion angles as compared to membrane bound state at specific residues (Val26 and Glu28) near the site of mutation. The WT α-Syn protein has been reported to display torsion angles for all residues that are close to that of a typical α-helix (phi (ϕ)~ -62 degrees and psi (ψ)~ - 41degrees) [467]. **Figure 6.22(A)** and **6.22(B)** depicts lower conformational changes to the helical structure, most notably at the Val26 (ϕ~ -25, ψ~ -75 degrees) and Glu28 (ϕ~ -100, ψ~ -98 degrees) positions as compared to A30G α-Syn in free monomer (**Figure 6.22(C)** and **6.22(D)**). The substantial changes are induced due to the addition of Glycine residue at 30^{th} position of α-Syn. The structural variation of A30G α-Syn in membrane bound and in free form as a function of simulation time depicts the dynamics along with the folding, unfolding and helical formation in the structure. From **Figure 6.22(C)** and **Figure 6.22(D)**, the torsion angles at the residue 26 (ϕ~ -125, ψ~ +25 degrees) and at the residue 28 (ϕ~ -150, ψ~ +150 degrees) indicate likely unfolding of the A30G α-Syn in free monomer form. **Figure 6.23** illustrates the different conformations of the A30G α-Syn in membrane bound form and free form.

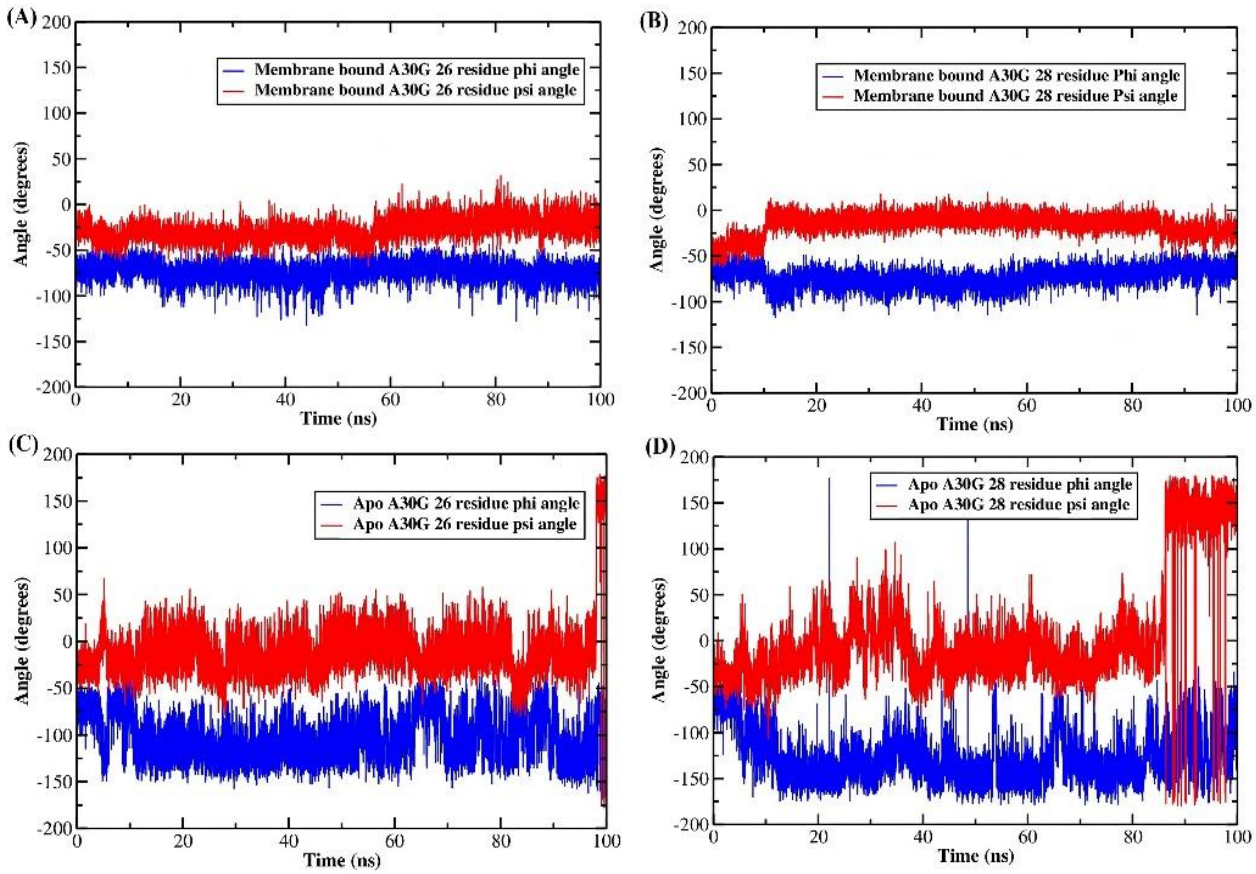

Figure 6.22. *Torsion angle analysis for the A30G α-Syn in (A-B) membrane bound form and (C-D) free monomeric form for the residues 26 and 28 as a function of simulation time*

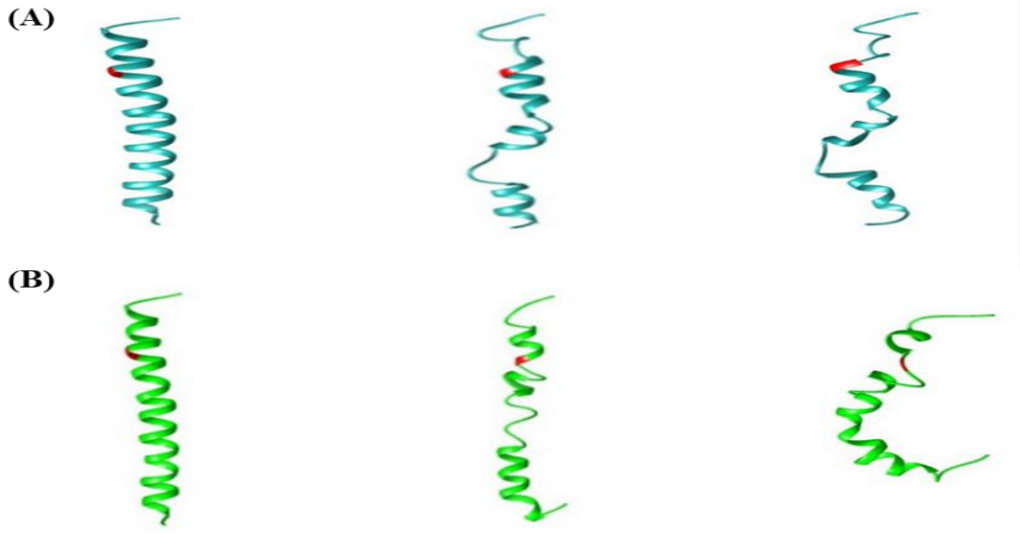

Figure 6.23*. Snapshots showing different conformations of the (A) membrane bound A30G α-Syn and (B) A30G α-Syn in free monomer form during the simulation time*

6.4.13. Prediction of α-Synuclein protein stability changes and functioning upon mutation:

To predict the stability of the WT α-Syn protein upon A30G mutation, ΔΔG value in kcal/mol was calculated from the online servers: I-Mutant 2.0, CUPSAT, MuPro, Dynamut, Auto-mute, SDM, and Prem PS. The results obtained from the servers have been summarized in the **Table 6.3**. According to **Table 6.3**, the ΔΔG value acquired from many servers was found to be negative, indicating that the A30G mutation reduces the stability of the WT α-Syn.

Table 6.3. *ΔΔG values upon single point mutation (A30G) in α-Syn*

Name of the Server	ΔΔG VALUE (kcal/mol)
I-mutant	-1.10
CUPSAT	-0.49
MuPRO	-2.019
Dynamut	-0.016
Auto-mute	Decreased (ΔΔG < 0)
Site directed Mutator	-1.56
Prem PS	-0.52

SIFT is a sequence homology based tool that sorts intolerant from tolerant amino acid substitutions and predicts whether an amino acid substitution in a protein will have an impact on the normal function of the protein [282]. According to SIFT, threshold for intolerance is 0.05; less than 0.05 indicates intolerance and more than 0.05 indicates tolerance. Seq Rep is the percentage of sequences that include one of the fundamental amino acids. From **Table 6.4**, A30G mutation was calculated to be 0.00 which is less than threshold for intolerance (<0.05) and predicts A30G mutation impact the function of α-Syn protein.

Table 6.4. *SIFT analysis to predict the tolerance of a single mutation A30G on WT α-Syn*

Residue Number	Tolerance/ intolerance score	Tolerance (affect/no affect)	Sequence Rep	Predict not tolerated	Predict tolerated
30	0.00	Affect protein function	1	y w v t s r q p n l k i h g f e d c a	M

The physiochemical properties determined from the ExPASy ProtParam online tool for the WT α-Syn protein also account for the increase in instability upon A30G mutation. The instability score of the α-Syn protein was found to increase from 25.47 to 26.35 upon mutation. The aliphatic index (that accounts for stability of the protein across wide temperature range) was found to be higher in the WT (69.64) than in the A30G α-Syn (68.90). The percent intrinsic disorder determined from PONDR VLXT was found to be higher in A30G α-Syn (39.29 %) than in the WT α-Syn (37.14 %) (as shown in **Figure 6.24**).

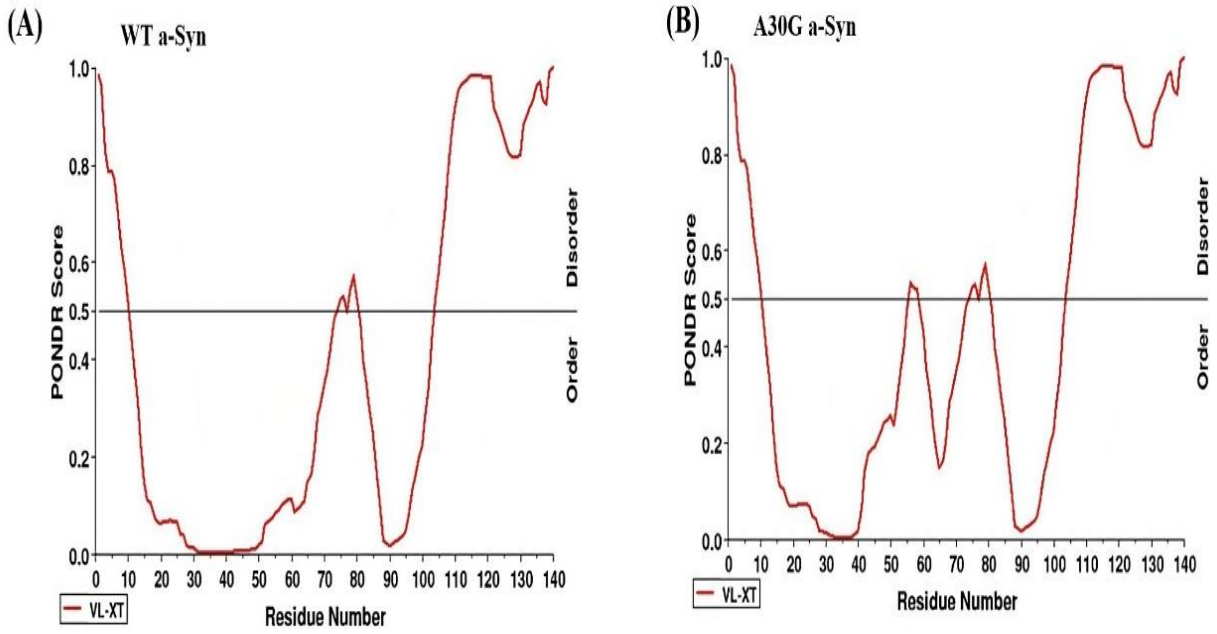

***Figure 6.24**. PONDR VLXT score calculated for (A) WT α-Syn and (B) A30G α-Syn in free monomer form during the simulation time*

6.5. Conclusion:

The structural dynamics of A30G α-Syn as a monomer in free solution and bound to the lipid membrane were compared using atomistic MD simulation in this study. In free solution, the structure of A30G α-Syn was found to be more flexible and less compact than the membrane bound form. In the membrane bound A30G α-Syn, paired lysine side chains point in opposite directions along the lipid bilayer surface and having impact on helical depth and topology. The helicity of membrane-bound A30G α-Syn was found to be more pronounced in the N-helix (3–37) and turn (38–44) regions, but helicity was shown to be significantly disrupted in the elevated regions above the lipid bilayer surface. The Cα RMSD and RMSF profile indicated the conformational stability in membrane bound A30G α-Syn than in the free monomer form.

Certain residues (Val26 and Glu28) close to the mutation site were shown to have considerably different typical α-helical torsion angles in both the free and membrane-bound forms of A30G α-Syn. But the total helical content was found to be relatively higher in the membrane-bound A30G α-Syn than in free form. The ΔΔG values obtained from different online servers, physiochemical properties (instability index, aliphatic index) determined from ExPASy online tool, the percent disorder calculated from PONDR VLXT predictor indicate the significant impact of A30G mutation on the stability and function of α-Syn protein. A30G α-Syn was also shown to have a larger bending angle in the helix-N and helix-C regions in its free form than in its membrane-bound state. The helical bending was found to exhibit a minor influence on the way the A30G α-Syn protein interacts with the membrane bilayer. We also found that rather than attaching evenly to membranes as a single entity, the different regions of α-Syn demonstrated diverse interaction modes. The key structural characteristics of A30G α-Syn addressed in this study may be helpful in understanding its function.